Applied Catalysis A, General 648 (2022) 118929

Contents lists available at ScienceDirect

Applied Catalysis A, General

journal homepage: www.elsevier.com/locate/apcata

Modulating multi-active sites in CeO_2-modified MnO_x/ZSM-5 catalyst for selective catalytic oxidation of diethylamine

Lin-Cong He, Xu-Fang Wang, Chu-Feng Liu, Bei Li, Meng-Fei Luo *, Jian Chen *

Key Laboratory of the Ministry of Education for Advanced Catalysis Materials, Zhejiang Key Laboratory for Reactive Chemistry on Solid Surfaces, Institute of Physical Chemistry, Zhejiang Normal University, Jinhua 321004, China

ARTICLE INFO

Keywords:
Catalytic oxidation
Internal selective catalytic reduction
MnO_x/CeO_2/ZSM-5 catalyst
Oxidation active site
Selective catalytic reduction (SCR) active sites
N_2 selectivity

ABSTRACT

An efficient MnO_x/CeO_2/ZSM-5 catalyst was developed for selective oxidation of diethylamine (DEA) with high N_2 selectivity in a wide temperature window ($\Delta T = 140$ °C), owing to the existence of oxidation and selective catalytic reduction (SCR) active sites. MnO_x species prefer to locate on the surface of CeO_2 compared to ZSM-5, and the presence of CeO_2 is beneficial to form more Mn^{4+} species, the active sites for oxidation reaction. The mechanistic investigation suggests that internal SCR of NO_x generated from the over-oxidized DEA is the crucial pathway for N_2 generation. The high SCR activity of the MnO_x/CeO_2/ZSM-5 catalyst in oxidation conditions is mainly attributed to the synergistic catalysis of Mn^{4+} species and acid sites of ZSM-5, the active sites for SCR reaction. Thus, it has been clearly clarified that addition of CeO_2 and its addition sequence could modulate the surface active sites of MnO_x/ZSM-5 catalyst for the selective catalytic oxidation of DEA.

1. Introduction

Nitrogen containing volatile organic compounds (NVOCs) tend to cause serious environmental pollution, thus, massive research efforts have been devoted to eliminate the NVOCs, including the adsorption, thermal combustion, catalytic combustion, etc [1–4]. The catalytic combustion is one of the most efficient strategies to transform NVOCs into harmless CO_2, H_2O and N_2. However, the challenge of this technology is how to avoid the formation of NO_x, a hazardous secondary pollutant, which is often generated by the over-oxidation of NVOCs. Numerous catalysts have been employed for the catalytic oxidation of NVOCs, including noble metal (Pt, Pd, Ru, etc.) and non-noble metal (Mn, Cu, Co, etc) catalysts [5–7]. Due to their high oxidation activities, the noble metal catalysts usually show excellent oxidation performance for C, H, or O containing VOCs, such as propane, toluene, ethyl acetate, and so on [8–11]. However, noble metal catalysts show very low N_2 selectivity for NVOCs oxidation, seriously limiting their application for NVOCs catalytic oxidation. As compared with the noble metal catalysts, transition metal oxides, such as MnO_x and CuO, based catalysts show much higher N_2 selectivity and thus have drawn more attentions for NVOCs catalytic oxidation [12–15]. Although non-noble metal catalysts have shown the promisingly potential applications for the NVOCs oxidation, the promotion in oxidation activity is always compromised by the deterioration in N_2 selectivity.

It was previously reported that supported MnO_x and CuO catalysts have not only been used for VOCs oxidation, but also for selective catalytic reduction (SCR) to transform NO_x into N_2 [16,17]. Wang et al. demonstrated that the promoted internal SCR activity greatly enhanced the N_2 selectivity for $CuCeO_x$-HZSM-5 catalyzed CH_3CN oxidation [18]. Our previous work also pointed out that the NO_x from over-oxidized DEA could be transformed into N_2 by further reacting with DEA or the DEA oxidation intermediate over CuO/SSZ-13 [13]. Thus, the fast transformation of NO_x from over-oxidized NVOCs to N_2 through SCR reaction is one of the important pathways for increasing the N_2 selectivity. However, the integration of SCR in oxidation of NVOCs and the relationship between SCR activity with N_2 selectivity have not been fully investigated. MnO_x-based catalysts generally have high SCR activity and they are potential catalysts for NVOCs oxidation [19–21]. The oxidation states of Mn species usually affect their catalytic performance for the SCR reaction, especially the N_2 selectivity. Mn^{4+} species with high oxidative ability have been considered as the key active sites for the SCR reaction [16,19]. Kapteljn et al. found that the oxidation degree of NH_3 to nitrogen containing products (N_2, N_2O and NO) depended on the oxidation state of Mn species in MnO_x catalyzed NH_3-SCR reaction [22]. In addition to the oxidation state of Mn species, the acid sites also have significant influences on SCR reaction [23–25]. Thus, it is necessary to

* Corresponding authors.
E-mail addresses: mengfeiluo@zjnu.cn (M.-F. Luo), jianchen@zjnu.cn (J. Chen).

https://doi.org/10.1016/j.apcata.2022.118929
Received 30 August 2022; Received in revised form 13 October 2022; Accepted 25 October 2022
Available online 30 October 2022

modulate both the oxidation state of Mn species and the acid sites for MnO_x-based catalysts to achieve high oxidation activity and high N_2 selectivity for NVOCs catalytic oxidation.

Herein, we reported the preparation of the MnO_x/CeO_2/ZSM-5 catalyst for the oxidation of diethylamine (DEA), a representative NVOCs. In the MnO_x/CeO_2/ZSM-5 catalyst with multi-active sites, CeO_2 assists the formation of more Mn^{4+} species, the catalytically active sites for the oxidation reaction, while ZSM-5 is responsible for providing acid sites. Thus, the synergy catalysis of Mn^{4+} species and the acid sites enables the internal SCR reaction to undergo smoothly to reduce NO_x from over-oxidation DEA, enhancing the oxidation activity and increasing N_2 selectivity. Based on the mechanistic investigation, the active sites for NVOCs oxidation and the reaction pathway for N_2 generation were clearly elucidated.

2. Experimental section

2.1. Reagents and chemicals

$Mn(NO_3)_2$ solution (50 wt%) was bought from Sinopharm Chemical Reagent Co. Ltd., China. $Ce(NO_3)_3{\cdot}6H_2O$ was obtained from Aladdin Reagent (Shanghai) Co., Ltd. ZSM-5 molecular sieve ($SiO_2/Al_2O_3 = 18$) was purchased from Shandong Dengzhuo Chemical Co., Ltd. China. Other reagents were of analytical grade and used without further purification.

2.2. Preparation of catalyst

Typical impregnation method was used for the preparation of MnO_x/ZSM-5 catalyst. ZSM-5 support was added to a desired amount of Mn $(NO_3)_2$ solution (mass ratio of Mn: ZSM-5 = 0.1). The mixture was stirred at 30 °C for 1 h before drying at 90 °C. After drying in an oven at 100 °C for 6 h, the solid was calcined at 400 °C for 2 h with a heating rate of 10 °C min^{-1}. The obtained catalyst was denoted as MnO_x/ZSM-5 catalyst. CeO_2/ZSM-5 catalyst with 40 wt% loading of CeO_2 was prepared with the similar procedure to that of MnO_x/ZSM-5. For the preparation of MnO_x/CeO_2 (10 wt% Mn), CeO_2 support was obtained by calcining $Ce(NO_3)_3{\cdot}6H_2O$ precursor at 400 °C. Other preparation procedures were also similar to the preparation of MnO_x/ZSM-5 catalyst.

MnO_x-CeO_2/ZSM-5 catalyst was prepared by co-impregnation of Mn $(NO_3)_2$ and $Ce(NO_3)_3{\cdot}6H_2O$ on ZSM-5 with similar procedure to that of the MnO_x/ZSM-5 catalyst. The content of Mn and CeO_2 in the catalyst are 10 and 20 wt%, respectively. And the oxides component are same to the dual oxides catalyst as described below.

MnO_x/CeO_2/ZSM-5 catalyst was prepared by sequential impregnation of CeO_2 and MnO_2 on ZSM-5. CeO_2 component was firstly loaded on the ZSM-5 by the typical impregnation method and CeO_2/ZSM-5 catalyst was obtained, then MnO_x component was loaded on CeO_2/ZSM-5 by the same impregnation method.

For the preparation of CeO_2/MnO_x/ZSM-5 catalyst, the impregnation order of CeO_2 and MnO_2 on ZSM-5 was adverse to that of MnO_x/CeO_2/ZSM-5 catalyst.

2.3. Characterization

N_2 adsorption measurement of catalyst was performed at 77 K on a BK200C system volumetric adsorption analyzer (Beijing Jingwei Gaobo Sci.-Tech. Ltd, Beijing, China). Prior to the sorption measurements, the catalyst was degassed at 120 °C for 12 h. The Brunauer-Emmett-Teller (BET) surface area was obtained from the adsorption data at a relative pressure (P/P_0) in the range of 0.05–0.35. The powder X-ray diffraction (XRD) patterns of catalysts were recorded using a Bruker D8 diffractometer using Cu Kα radiation with a scan speed of 12° min^{-1} from 2θ of 10–90°, operating at 40 kV and 40 mA. Field emission scanning transmission electron microscope (FE-STEM) images and Energy dispersive spectrometer (EDS) analysis were obtained on JEOL-2100F instrument operated at 200 kV. H_2-temperature programmed reduction (H_2-TPR) experiments were conducted on a lab-made tubular quartz reactor (*i.d.* = 6 mm) equipped with a thermal conductivity detector (TCD). In typical, 35 mg of catalyst was put in the reactor and heated from 30 to 800 °C with a heating ramp of 20 °C min^{-1} (in a flow of 5 % H_2 + 95 % N_2, 30 mL min^{-1}). The signal of gas was recorded using a TCD detector after the H_2O elimination by solid KOH fixed in a quartz tube. X-ray photoelectron spectra (XPS) were recorded on an ESCALAB 250Xi instrument with Al K_α source ($h\nu = 1486.6$ eV). The binding energies (BEs) was calibrated by the carbonaceous C1s line (284.6 eV). Surface acidity of the catalyst was measured by the temperature-programmed desorption of NH_3 (NH_3-TPD) under a fixed-bed reactor equipped with a mass spectrometer (MS) Ominstar 300. Before measurement, 200 mg of catalyst (60–80 mesh) was heated in He flow (20 mL min^{-1}) from 30 to 300 °C (10 °C min^{-1}) and kept at 300 °C for 30 min, and then cooled to 100 °C. Afterward, a flow of 10 % NH_3 + 90 % He (30 mL min^{-1}) was introduced to the reactor for 10 min at 50 °C for NH_3 adsorption on the catalyst. The gaseous or physically adsorbed NH_3 was removed by purging with a He flow (20 mL min^{-1}) for 30 min before the MS detector measurement. Finally, the catalyst was heated in the He flow (20 mL min^{-1}) from 40 to 700 °C at a rate of 10 °C min^{-1}, and the desorption of NH_3 was detected by MS detector.

2.4. Activity evaluation

2.4.1. Diethylamine (DEA) oxidation

The catalytic activity of catalysts for DEA oxidation was performed in a home-made quartz tubular reactor (*i.d.* = 8 mm) with 1 mL catalyst (20–40 mesh, 0.45 g) at atmospheric pressure. A air flow of 5 mL min^{-1} was flowed into a bottle with liquid DEA at 0 °C, and then the saturated DEA vapor flow (5 mL min^{-1}) was diluted by another air flow of 300 mL min^{-1}. The mixture gas consisted of ca. 4200 mg m^{-3} DEA was inlet into reactor with a mass space velocity (S.V.) of 20, 000 mL g^{-1} h^{-1}. DEA vapor concentration was determined by an online gas chromatography (Shimadzu GC-2014) equipped with a flame ionization detector (FID) and an SH-Stabliwax-DB capillary column (30 m × 0.32 mm). DEA conversion can be calculated by the following equation:

$$\text{Conversion} = ([C]_{in} - [C]_{out})/[C]_{in} \times 100\ \%$$

Where $[C]_{in}$ and $[C]_{out}$ are DEA concentrations in the inlet and outlet gas, respectively.

NO_x and CO were analyzed by flue gas analyzer (ecom-EN3, ECOM, Germany), and no NH_3 was detected. The selectivity of N_2 was calculated by the following equation:

$$Selectivity\ (N_2) = \left(1 - \frac{\text{actualNOxyield}}{\text{theoreticalNOxyield}}\right) \times 100\%$$

Simultaneously, the selectivity of CO is also calculated by the ratio of actual CO concentration and theoretical CO concentration.

2.4.2. Diethyl ether (DE) oxidation reaction

The process of DE oxidation activity evaluation is the same to that of DEA mentioned above. The gaseous DE concentration is 8800 mg m^{-3} DE. Other procedures were the same to DEA oxidation reaction.

2.4.3. Standard NH_3-SCR reaction

The NH_3-SCR activity test was performed in a fixed-bed reactor with 0.5 mL catalyst (50–80 mesh). Prior to the test, the sample was pretreated at 500 °C in 20 % O_2/N_2 (100 mL min^{-1}) for 0.5 h to remove adsorbed impurities. Then, a mixture gas (500 ppm NO, 500 ppm NH_3 and 5 % O_2, with N_2 as balance gas) was passed through the catalyst bed with a mass space velocity (S.V.) of 110,000 mL g^{-1} h^{-1}. The gas components were measured by infrared (IR) spectroscopy on a Nicolet iS50 spectrometer (Thermo Fisher, USA), and the background spectrum was collected in N_2 at each desired temperature.

3. Results and discussion

3.1. Catalytic performance of Mn-based catalysts for DEA oxidation

The catalytic performance of MnO_x-based catalysts has been evaluated in DEA oxidation (Fig. 1 and Table 1). The MnO_x/ZSM-5 catalyst shows a moderate activity for DEA oxidation with T_{99} (the reaction temperature with DEA conversion of 99 %) of 280 °C, but the CeO_2/ZSM-5 catalyst exhibits T_{99} of 380 °C, suggesting that MnO_x species are more active than CeO_2 species for DEA oxidation. The MnO_x/CeO_2/ZSM-5, MnO_x-CeO_2/ZSM-5 and CeO_2/MnO_xZSM-5 catalysts show higher oxidation activity than the bare MnO_x/ZSM-5 catalyst for DEA oxidation, for example, the MnO_x-CeO_2/ZSM-5 catalyst shows a T_{99} of only 230 °C. The MnO_x/CeO_2 catalyst with T_{99} of only 190 °C is more active than others for DEA oxidation. The above results suggest that CeO_2 promoted the oxidation activity of the MnO_x/ZSM-5 catalyst for DEA oxidation.

In addition to the oxidation activity, the selectivities to CO and N_2 are also important performance indicators to evaluate a catalyst for NVOCs oxidation. For CO selectivity, the CeO_2/ZSM-5 catalyst exhibits the highest CO selectivity which is ascribed to its lowest oxidation activity. For instance, the CeO_2/ZSM-5 and MnO_x/ZSM-5 catalysts show the CO selectivity of 9.2 % and 0.3 % at 300 °C, respectively. No CO could be detected in the outlet for the duel oxides catalysts at 300 °C (MnO_x/CeO_2/ZSM-5, MnO_x-CeO_2/ZSM-5 and CeO_2/MnO_x/ZSM-5). And the MnO_x/CeO_2 catalyst shows the lowest selectivity to CO among these catalysts in the measured temperature range. Such findings further confirm that CeO_2 promoted the oxidation activity of MnO_x species. For N_2 selectivity, the MnO_x/CeO_2 catalyst, having the highest oxidation activity, exhibits the lowest N_2 in comparison with single oxide catalysts of MnO_x/ZSM-5 and CeO_2/ZSM-5, or dual oxides catalysts of MnO_x/CeO_2/ZSM-5, MnO_x-CeO_2/ZSM-5 and CeO_2/MnO_x/ZSM-5. Compared to the CeO_2/ZSM-5 catalyst, the MnO_x/ZSM-5 catalyst with a higher oxidation activity shows a much higher N_2 selectivity. The results above suggest that strong oxidation active sites supported on ZSM-5 could present a high N_2 selectivity for the DEA oxidation. To clearly understand the changes of N_2 selectivity in these catalysts, temperature window (ΔT) for high N_2 selectivity has been analyzed. ΔT represents the temperature range after T_{99} in which N_2 selectivity is higher than 99 %. The narrowest temperature window is observed on the MnO_x/CeO_2 catalyst with ΔT of 10 °C. Temperature window of MnO_x-based catalyst could be remarkably broadened when MnO_x component is loaded on the ZSM-5, as seen in the MnO_x/ZSM-5 catalyst with ΔT of 60 °C. Addition of CeO_2 species in the MnO_x/ZSM-5 catalyst further broadens the ΔT, and its addition sequence also significantly affects the ΔT of the obtained catalysts. Among the MnO_x/CeO_2/ZSM-5, MnO_x-CeO_2/ZSM-5 and CeO_2/MnO_x/ZSM-5 catalysts, the MnO_x/CeO_2/ZSM-5 catalyst has the widest ΔT of 140 °C. The effect of CeO_2/ZSM-5 ratio on

Table 1
The T_{99}, selectivity of N_2 and CO at T_{99} and temperature window ΔT for high N_2 selectivity of DEA oxidation over MnO_x-based catalysts.

Catalyst	T_{99}[a]/ °C	S_{CO}[b]/ %at T_{99}	CO concentration/ ppm at T_{99}	S_{N2}[c]/ %at T_{99}	T_{N2}[d]/ °C	ΔT[e] = T_{N2}-T_{99}/°C
MnO_x/CeO_2	190	0	0	100	200	10
MnO_x/ZSM-5	280	0.9	11.4	100	340	60
CeO_2/ZSM-5	380	2.25	68.7	100	400	20
MnO_x-CeO_2/ZSM-5	230	0	0	100	340	110
MnO_x/CeO_2/ZSM-5	220	0	0	100	360	140
CeO_2/MnO_x/ZSM-5	250	0	0	100	380	130

[a] T_{99}: the temperature for DEA conversion of 99 %.
[b] S_{CO}: the CO selectivity.
[c] S_{N2}: the N_2 selectivity.
[d] T_{N2}: the highest temperature for N_2 selectivity of 99 %.
[e] ΔT: the temperature window for high N_2 selectivity (> 99 %).

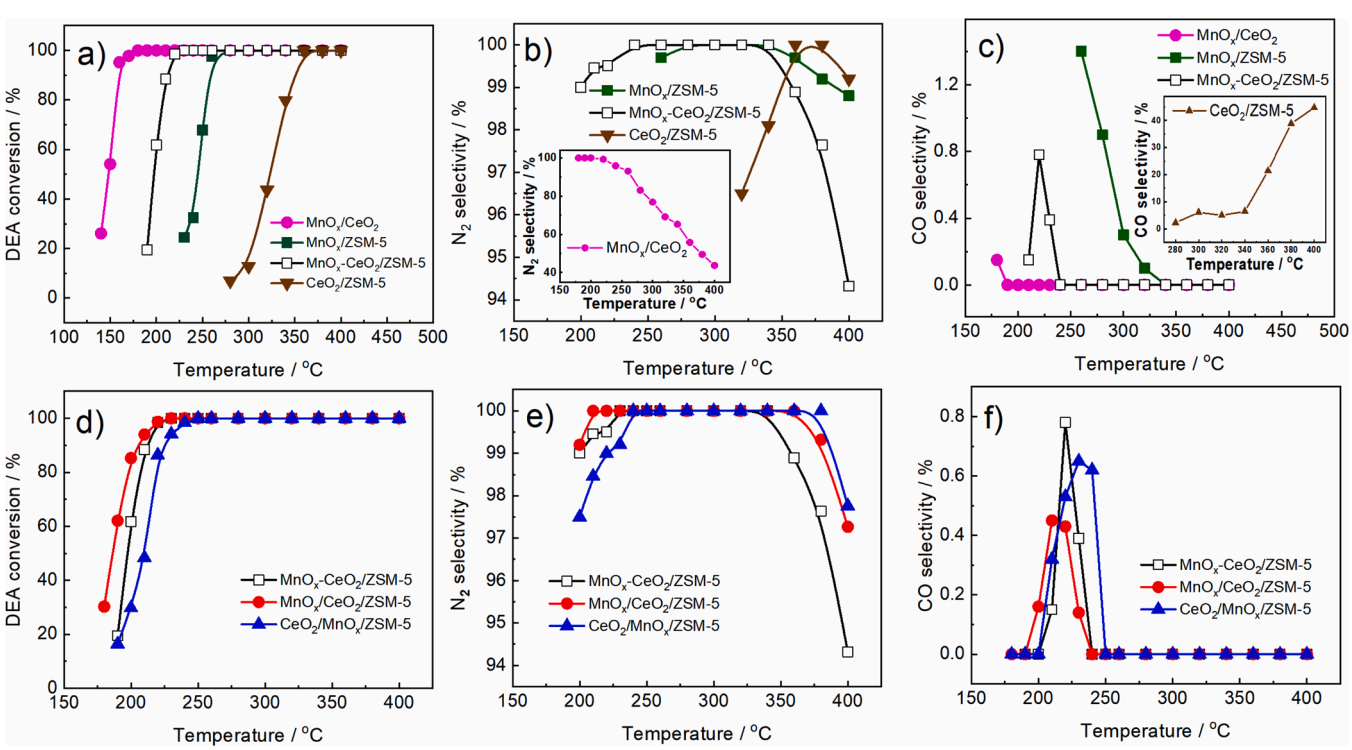

Fig. 1. The catalytic performance of MnO_x-based catalysts for the DEA oxidation.

the catalytic performance has been further studied (Fig. S1). Catalytic oxidation activity of MnO_x/CeO_2/ZSM-5 catalyst gradually increases with the increase of CeO_2/ZSM-5 ratio from 1/9 to 2/3, confirming the promotion of CeO_2 specie on oxidation activity. The oxidation activity of MnO_x/CeO_2/ZSM-5 catalyst decreases when the CeO_2/ZSM-5 ratio further is increased 1/1. Considering to develop a catalyst with wide temperature window for high N_2 selectivity after complete DEA oxidation, it can be seen that the MnO_x/CeO_2/ZSM-5 catalyst with CeO_2/ZSM-5 ratio of 1/4 shows the widest temperature window of 140 °C which will be further discussed in following. The results above confirm that the CeO_2 species could not only improve the oxidation activity but also the N_2 selectivity of the MnO_x/ZSM-5 catalyst for DEA oxidation.

3.2. Characterizations of the catalysts

The specific surface areas of all catalysts are summarized in Table 2. The MnO_x/CeO_2 catalyst shows very low surface area of 86 m^2/g. CeO_2 and MnO_x oxides supported on ZSM-5 has relatively higher surface areas because of the high surface area of ZSM-5 support (ca. 340 m^2/g). The CeO_2/ZSM-5 catalyst has the highest surface area of 229 m^2/g even with high CeO_2 content of 40 wt%, but the MnO_x/ZSM-5 catalyst only has a surface area of 167 m^2/g. For the CeO_2-modified MnO_x/ZSM-5 catalysts, the addition sequence of CeO_2 also significantly affects the surface areas of obtained catalysts. Among them, the BET surface area of the MnO_x/CeO_2/ZSM-5 catalyst is much higher than that of the MnO_x-CeO_2/ZSM-5 catalyst (210 vs. 146 m^2/g). It could be inferred that major CeO_2 species locate on the surface of ZSM-5 whereas MnO_x species may be filled into the pores of ZSM-5.

The XRD patterns of all ZSM-5 supported catalysts display the characteristic diffraction peaks assigned to ZSM-5 at 2-theta of 23°, 24°, 30° and 45° (JCPDS no. 44-0003) in Fig. 2, implying well retained ZSM-5 for the supported catalysts. The characteristic diffractions at 2-theta of 28.5°, 33.1°, 47.5° and 56.3° ascribed to the cubic phase CeO_2 (JCPDS no. 81-0792) appear in the XRD patterns of the MnO_x/CeO_2, MnO_x/CeO_2/ZSM-5 and CeO_2/MnO_x/ZSM-5 catalysts. But very weak diffractions assigned to CeO_2 phase are observed in the XRD patterns of the MnO_x-CeO_2/ZSM-5 catalyst prepared by Mn and Ce co-impregnation, suggesting the generation of smaller size or amorphous CeO_2 species. The CeO_2 crystallite sizes of the MnO_x/CeO_2, MnO_x/CeO_2/ZSM-5 and CeO_2/MnO_x/ZSM-5 catalysts calculated by Scherrer equation is 6.4, 6.9, and 6.8 nm, respectively, suggesting the sequence hardly affects the size of CeO_2. The absence of characteristic diffractions corresponding to

Table 2
The surface area, CeO_2 size, relative reduction peak area and ratio of reduction peak area of the MnO_x-based catalysts.

Catalyst	BET surface area[a]/m^2 g^{-1}	CeO_2 size[b]/nm	Relative reduction peak area[c]	Ratio of reduction peak area (α/β)
MnO_x/ZSM-5	167	–	1	0.8
MnO_x/CeO_2	86	6.4	2.1	1.7
CeO_2/ZSM-5	229	7.7	–	–
MnO_x-CeO_2/ZSM-5	146	–	1.6	1.5
MnO_2/CeO_2/ZSM-5	210	6.9	1.6	1.6
CeO_2/MnO_2/ZSM-5	156	6.8	1.5	1.4

[a] BET surface area was measured by N_2 adsorption at 77 K.
[b] CeO_2 crystallite size was calculated by Scherrer equation.
[c] Relative reduction peak area in H_2-TPR profiles was obtained with reference to the MnO_x/ZSM-5 catalyst.

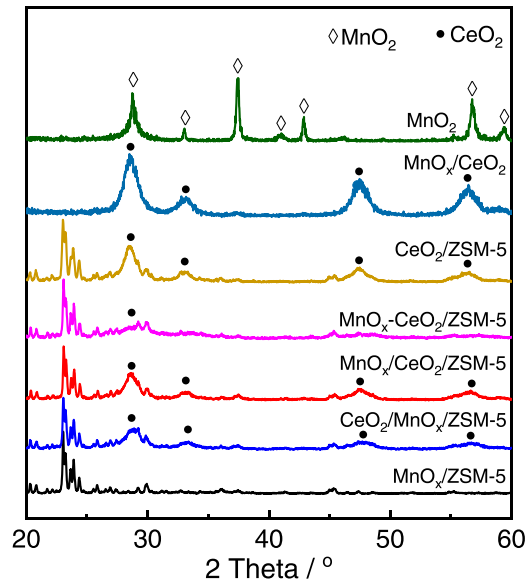

Fig. 2. XRD patterns of the MnO_2, MnO_x/CeO_2, CeO_2/ZSM-5, MnO_x-CeO_2/ZSM-5, MnO_x/CeO_2/ZSM-5 and CeO_2/MnO_x/ZSM-5 catalysts.

MnO_x signifies the amorphous phase of MnO_x in all the catalysts [14].

Fig. 3 displays the H_2-TPR profiles of the MnO_x-based catalysts to investigate their reducibilities. Remarkable reduction peaks appear in the H_2-TPR profiles of all the MnO_x containing catalysts and no reduction peaks could be observed for the CeO_2/ZSM-5 catalyst, suggesting the reduction peaks are mainly assigned to MnO_x and reduction of CeO_2 is negligible. For the MnO_x/ZSM-5 catalyst, there are two apparent reduction peaks at 330 °C (α) and 440 °C (β). According to the previous report that MnO is the final state of MnO_x reduction [22], the reduction process of MnO_x could be described by the following expressions:

$$MnO_2 \xrightarrow{\frac{2}{3}H_2} \frac{1}{3}Mn_3O_4 + \frac{2}{3}H_2O \xrightarrow{\frac{1}{3}H_2} MnO + H_2O \quad (1)$$

$$\frac{1}{2}Mn_2O_3 \xrightarrow{\frac{1}{6}H_2} \frac{1}{3}Mn_3O_4 + \frac{1}{6}H_2O \xrightarrow{\frac{1}{3}H_2} MnO + \frac{1}{2}H_2O \quad (2)$$

Thus, the peak α centered at 330 °C is ascribed to the reduction of MnO_2 or Mn_2O_3 to Mn_3O_4, whereas the peak β centered at 440 °C corresponds to the subsequent reduction of Mn_3O_4 to MnO [22,26,27].

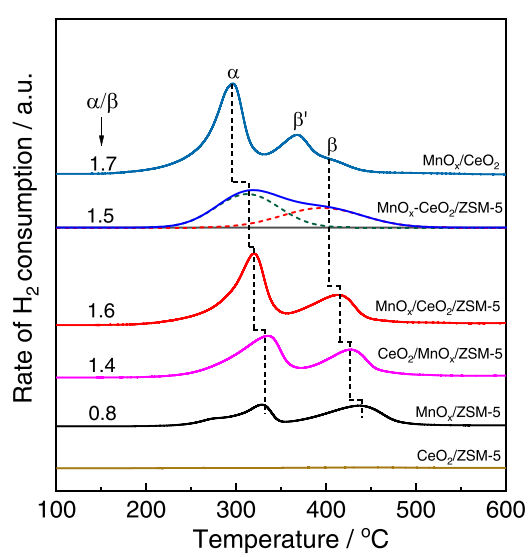

Fig. 3. The H_2-TPR profiles of the MnO_x-based catalysts.

These two reduction peaks of the MnO_x/CeO_2 catalyst shift to lower temperatures compared to those of the MnO_x/ZSM-5 catalyst, indicating that CeO_2 facilitates the reduction of MnO_x. Similar tendency is observed for the MnO_x-CeO_2/ZSM-5 and MnO_x/CeO_2/ZSM-5 catalysts. Different from the other dual oxides catalysts, the CeO_2/MnO_x/ZSM-5 catalyst has similar reduction temperature to those of the MnO_x/ZSM-5 catalyst, implying the different distributions of Mn and Ce in this catalyst from others.

Relative reduction peak area of these catalysts in H_2-TPR profiles were evaluated by referencing the MnO_x/ZSM-5 catalyst (Table 2). The reduction peaks area of the CeO_2 modified MnO_x/ZSM-5 catalysts are increased in comparison with the that of the MnO_x/ZSM-5 catalyst, and the MnO_x/CeO_2 catalyst shows the highest relative reduction peak area of 2.1. Considering the negligible reduction of CeO_2 species, the increased relative reduction peak area indicates more Mn^{4+} species in this catalyst. In addition, the ratio of reduction peak α/β is also analyzed, the theoretical ratio of α/β is 2 or 0.5 for a catalyst with the assumption of pure MnO_2 or Mn_2O_3 phase in the catalyst according to the expressions (1) and (2), respectively. The MnO_x/ZSM-5 catalyst shows a ratio of α/β to 0.8, implying that Mn^{3+} is the major species in the catalyst. Whereas the ratio of α/β in CeO_2 modified MnO_x/ZSM-5 catalyst increases to 1.4–1.6, suggesting more Mn^{4+} species generated in the catalyst. The MnO_x/CeO_2 catalyst shows the highest ratio of α/β to 1.7, implying that it has the most Mn^{4+} species. Such finding also suggests that CeO_2 promotes the generation of more MnO_x species in the high oxidation state (Mn^{4+}). According to the ratio of α/β, it could be inferred that the amount of Mn^{4+} species in the catalysts is in the order of MnO_x/CeO_2 > MnO_x/CeO_2/ZSM-5 > MnO_x-CeO_2/ZSM-5 > CeO_2/MnO_x/ZSM-5 > MnO_x/ZSM-5. The above observations certainly suggest that CeO_2 species could modulate the oxidation state of Mn species, leading to the generation of more Mn^{4+} species.

The XPS technique was employed to further investigate the surface MnO_x and CeO_2 species of these catalysts (Fig. 4, and Table 3). For the deconvoluted spectra (Fig. 4a), the Mn2p$_{3/2}$ binding energies at 641.3 and 642.5 eV are attributed to Mn^{3+} and Mn^{4+} species, respectively [14]. The peak with binding energy at 644.4 eV is assigned to the satellite peak of Mn 2p$_{3/2}$ [14]. All the CeO_2 modified MnO_x/ZSM-5 catalysts showed higher content of surface Mn^{4+} species compared to the MnO_x/ZSM-5 catalyst (Table 3). For example, the MnO_x/CeO_2/ZSM-5 catalyst has a surface Mn^{4+} content of 78.6 %, higher than 60.7 % for the MnO_x/ZSM-5 catalyst. And the MnO_x/CeO_2 catalyst has the highest surface Mn^{4+} content of 80.7 % among all these catalysts. These results confirm that more Mn^{4+} species would be generated on the surface of CeO_2 species, which is also consistent with the H_2-TPR results (Fig. 3).

For the deconvoluted Ce 3d spectra (Fig. 4b), the peaks denoted to "v" correspond to component of Ce 3d$_{5/2}$ spectra, while those categorized as "u" represents the component of Ce 3d$_{3/2}$ spectra. The peaks of v′ (884.4 eV) and u′ (903.3 eV) could be assigned to the Ce 3d$_{5/2}$ and 3d$_{3/2}$ spectra of Ce^{3+} species, while other peaks are attributed to the Ce 3d$_{5/2}$ (v: 882.7 eV; v'': 888.9 eV; v''': 898.7 eV) and 3d$_{3/2}$ (u: 901.3 eV; u'': 907.8 eV; u''': 917.0 eV) spectra of the Ce^{4+} species, suggesting the multiple oxidation states of Ce species in the catalysts [28–31]. As shown in Table 3, the Ce^{4+} species are much more than Ce^{3+} species, suggesting Ce^{4+} dominated in the CeO_2 lattice. The appearance of Ce^{3+} species represents the existence of oxygen vacancies on the catalyst surface. Thus, the ratio of Ce^{3+}/Ce^{4+} has been evaluated. The MnO_x/-CeO_2/ZSM-5 catalyst shows the highest ratio of ratio of Ce^{3+}/Ce^{4+} (0.21) among the catalysts, indicating the most abundant oxygen vacancies in the MnO_x/CeO_2/ZSM-5 catalyst [18,19].

Surface atomic ratio of Mn/Ce for the Mn and Ce dual oxides catalysts has been estimated from XPS result (Table 3). The MnO_x/CeO_2 catalyst shows a surface atomic ratio of Mn/Ce of 0.5, which is much higher than the theoretical value of 0.3 (weight ratio of Mn/CeO_2 = 1/10 in MnO_x/CeO_2). For the three CeO_2-modified MnO_x/ZSM-5 catalysts (MnO_x-CeO_2/ZSM-5, MnO_x/CeO_2/ZSM-5 and CeO_2/MnO_x/ZSM-5), the theoretical surface atomic ratio of Mn/Ce is 0.8 (weight ratio of Mn/CeO_2 = 1/4 in these catalysts). However, only the CeO_2/MnO_x/ZSM-5 catalyst shows an actual surface atomic Mn/Ce ratio close to the theoretical value of 0.8. The MnO_x-CeO_2/ZSM-5 and MnO_x/CeO_2/ZSM-5 catalysts show actual surface atomic Mn/Ce ratios of 1.7 and 1.9, respectively, which are two folds higher than the theoretical value. Therefore, it could be inferred that MnO_x species prefer to locate on the CeO_2 surface in co-impregnation or MnO_x species later impregnation method, thereby presenting an atomic ratio of Mn/Ce exceeding the theoretical value.

The O1s spectra has been analyzed for discussing the surface oxygen species (Fig. 4c, Table 2). Lattice oxygen species assigned to MnO_2 and ZSM-5 were calibrated by pure MnO_2 oxides derived from calcining Mn $(NO_3)_2$ and ZSM-5 support, respectively. In the O1s spectra, the components with binding energy at 532.6 (O_a), 529.9 (O_c) and 529.3 (O_d) eV are attributed to the lattice oxygen of ZSM-5, MnO_x and CeO_2, respectively [32–34]. O_b component is assigned to the surface absorbed oxygen including the carbonates, hydroxyl groups, and the binding energy of O_b varies with the type of oxides [18,19,32,33]. It is widely recognized that the high ratio of surface absorbed oxygen (O_b) represents more oxygen vacancies. Therefore, the content of oxygen vacancy in these catalyst are ordered as follows: MnO_x/CeO_2 > MnO_x/CeO_2/ZSM-5 > CeO_2/MnO_x/ZSM-5 > CeO_2-MnO_x/ZSM-5 > -MnO_x/ZSM-5.

Fig. 5 shows the HAADF-STEM-EDX element-mapping images of

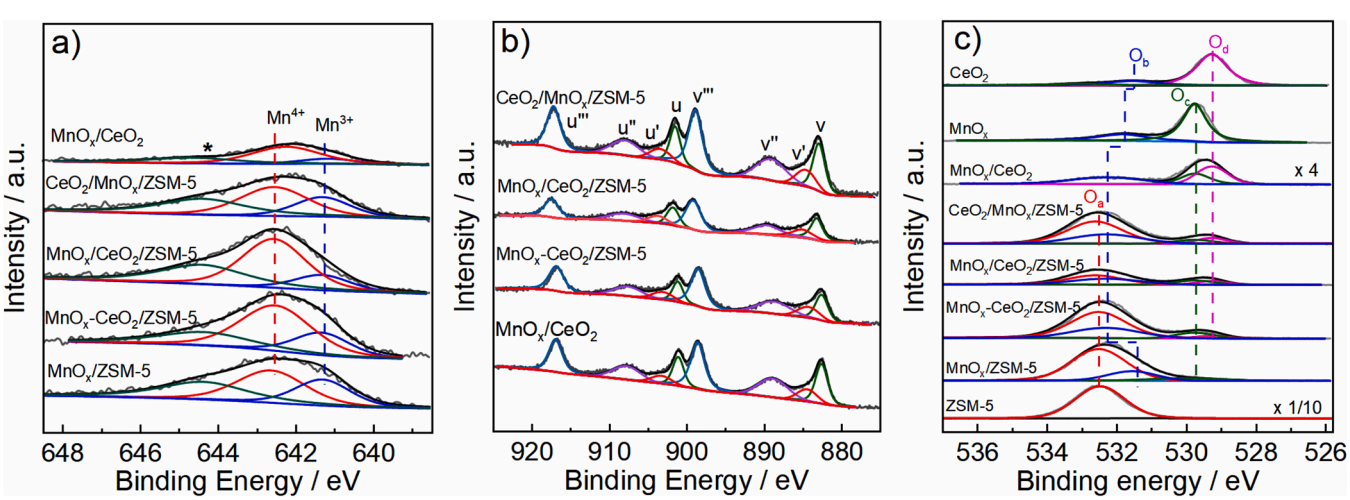

Fig. 4. The XPS spectra of a) Mn2p3/2, b) Ce 3d and c) O1s of the MnO_x-based catalysts.

Table 3
The surface Mn, Ce and O element chemical states, and surface atomic Mn/Ce ratio of the MnO_x-based catalysts.

Catalyst	Mn^{3+} (%)	Mn^{4+} (%)	Mn^{4+}/Mn^{3+}	Ce^{3+} (%)	Ce^{4+} (%)	Ce^{3+}/Ce^{4+}	Theoretical surface atomic ratio Mn/Ce	Actual atomic surface ratio Mn/Ce	O_a (%)	O_b (%)	O_c (%)	O_d (%)
MnO_x/ZSM-5	39.3	60.7	1.5	–	–	–	–	–	73.3	18.8	7.9	–
MnO_x/CeO_2	19.3	80.7	4.2	10.9	89.1	0.12	0.3	0.5	–	35.2	25.4	39.3
MnO_x-CeO_2/ZSM-5	28.1	71.9	2.6	14.0	86.0	0.16	0.8	1.7	61.9	26.3	8.4	3.4
MnO_x/CeO_2/ZSM-5	21.4	78.6	3.6	17.8	82.2	0.21	0.8	1.9	45.9	31.7	13.0	9.4
CeO_2/MnO_x/ZSM-5	35.0	65.0	1.9	12.2	87.8	0.14	0.8	0.8	59.0	26.8	6.4	7.8

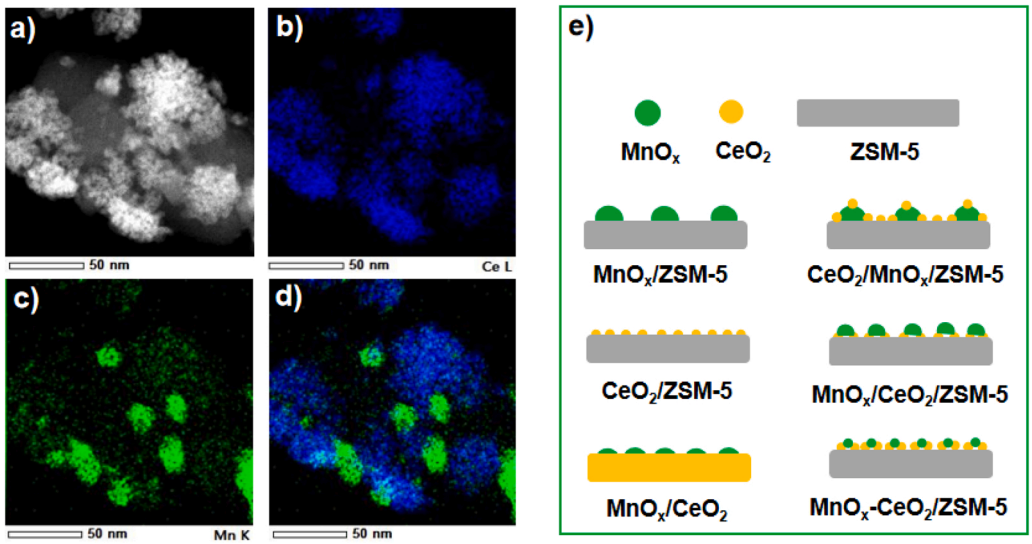

Fig. 5. a–d) STEM and elements mapping images of MnO_x/CeO_2/ZSM-5 catalyst, e) The possible distribution of Mn and Ce oxides in the catalysts.

representative catalyst of MnO_x/CeO_2/ZSM-5, and the possible distribution of MnO_x and CeO_2 in the catalysts. It can be seen that Ce element (blue color) is uniformly dispersed on the surface of catalyst, and major MnO_x species locate on the CeO_2 surface in the MnO_x/CeO_2/ZSM-5 catalyst (Fig. 5a). Based on the surface atomic ratio of Mn/Ce from XPS spectra, the possible model of MnO_x and CeO_2 distribution on catalysts are provided in Fig. 5b. CeO_2 species could locate on both the surface of ZSM-5 or MnO_x, whereas the MnO_x species prefer to locate and enrich on the surface of CeO_2 rather than on ZSM-5.

Fig. 6 displays the NH_3-TPD profiles of the catalysts. Firstly, remarkable NH_3 desorption peaks are observed for all these catalysts except for the MnO_x/CeO_2 catalyst, suggesting that the acid sites are mainly from ZSM-5 support. The peaks of NH_3 centered in temperature range of 100–200 °C are ascribed to NH_3 desorption from the weak acid sites, and the peaks in the temperature range of 200–400 °C correspond to the moderate strong acid sites [13–15,35]. However, the shapes and temperatures of NH_3 desorption peaks determined by MS detector in this work seem to be very different to those measured by TCD detector for the similar catalysts (CuO/ZSM-5, MnO_x/ZSM-5) in our previous works [14,15], which is ascribed to that TCD cannot differentiate the NH_3 with other substances (NO, N_2 and H_2O). Secondly, the appearance of NO and N_2 peaks indicates the occurrence of redox reaction of NH_3 on the catalyst surface. Such finding also confirms the presence of oxidation active sites and SCR active sites in the MnO_x/ZSM-5 catalyst and the CeO_2-modified MnO_x/ZSM-5 catalysts. The increased SCR activities of catalysts at high temperature (ca. 300 °C) accounts for the formation of more N_2 [36]. Besides, the signal of N_2 is perfectly accompanied by H_2O, further confirming the occurrence of the SCR reaction.

It is necessary to identify the active sites of catalysts for the SCR reaction during NH_3-TPD. The MnO_x/CeO_2 catalyst only shows weak peaks of NO without NH_3, N_2 and H_2O observed (Fig. 6b) during NH_3-TPD, suggesting no occurrence of SCR reaction owing to the lack of acid sites. The absence of N_2 peak in the NH_3-TPD profile of bare ZSM-5 support represents SCR reaction cannot undergo on the catalyst containing only abundant acid sites without oxidation active sites (Fig. S1). Whereas the MnO_x/ZSM-5 catalyst shows the remarkable N_2 peak in the NH_3-TPD profile, even weak N_2 peaks are observed in the CeO_2/ZSM-5 catalyst, confirming that both the oxidation active sites (from MnO_x and/or CeO_2) and acid sites of ZSM-5 are indispensable for the SCR reaction during NH_3-TPD. Nanba et al. also found the N_2 and H_2O evolution during the NH_3-TPD over Cu-ZSM-5 catalyst, lattice oxygen of Cu-ZSM-5 catalyst could be regarded as the active sites [37]. Remarkable signals of NO but only weak ones of N_2 are observed for the CeO_2/ZSM-5 catalyst, suggesting the oxidation active sites from CeO_2 is enough to oxidize the NH_3 but still inefficient for undergoing SCR reaction. The MnO_x/ZSM-5 catalyst has more acid sites and higher oxidation activity compared to the CeO_2/ZSM-5 catalyst (Figs. 1 and 6), which should be responsible for the strong N_2 signal in NH_3-TPD observed on the MnO_x/ZSM-5 catalyst. Moreover, the oxidation activities of CeO_2-modified MnO_x/ZSM-5 catalysts have been further improved in comparison with the MnO_x/ZSM-5 catalyst (Fig. 1), and these catalysts also present the stronger N_2 signals in NH_3-TPD in comparison with the MnO_x/ZSM-5 catalyst. Among them, the MnO_x/-CeO_2/ZSM-5 catalyst having the highest oxidation activity shows the strongest N_2 signal in the NH_3-TPD profile, suggesting its highest SCR reactivity. Therefore, the above observations confirm that both strong oxidation active sites and abundant acid sites are crucial for a high SCR reactivity.

In order to directly understand the oxidation and SCR reactivities of the catalysts, model reactions of diethyl ether (DE) oxidation and

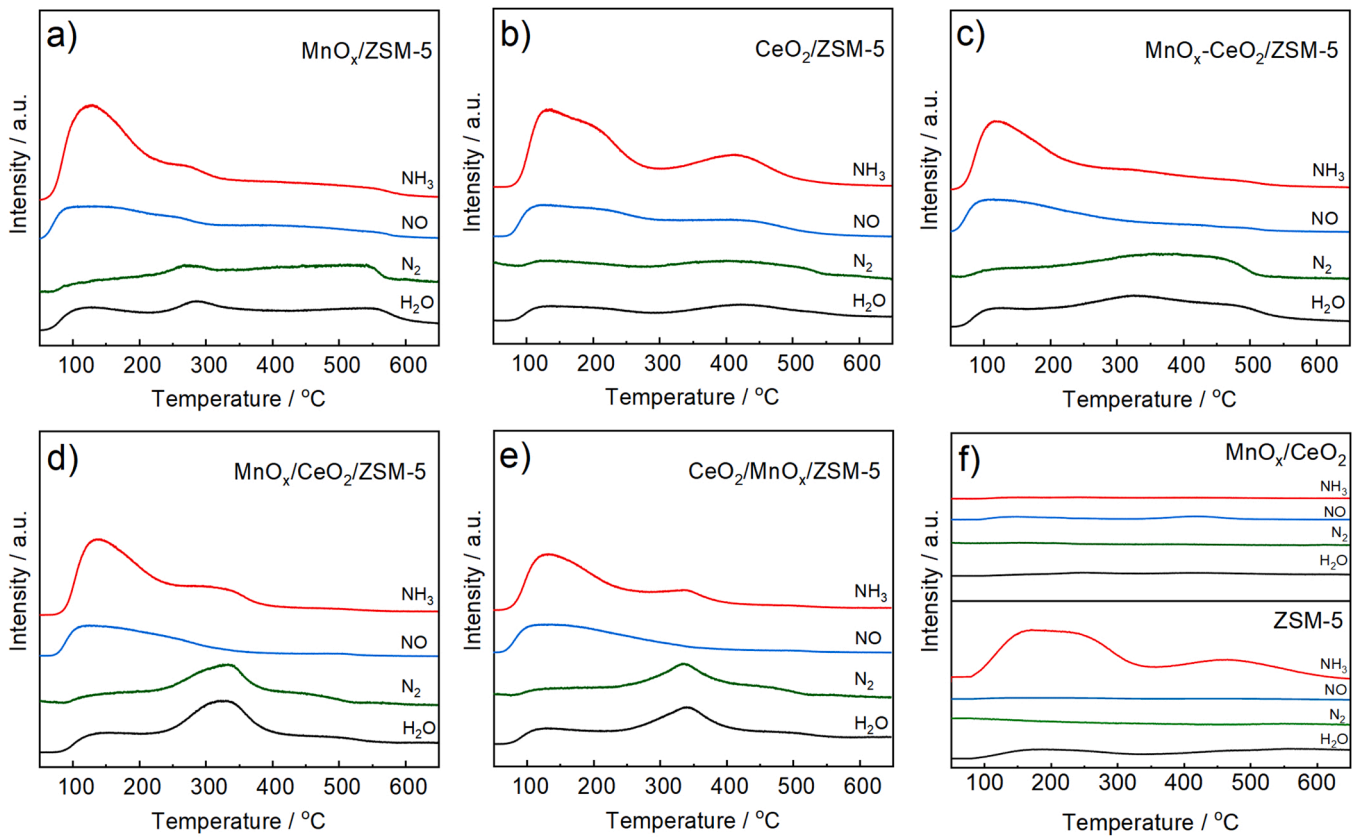

Fig. 6. The NH_3-TPD profiles of the MnO_x-based catalysts.

standard NH_3-SCR reaction have been conducted over the three representative catalysts (MnO_x/CeO_2, MnO_x/ZSM-5 and MnO_x/CeO_2/ZSM-5) as shown in Fig. 7. Oxidation reaction of DE with the similar structure of DEA has been employed to evaluate the oxidation reactivity of a catalyst, while the NH_3-SCR reaction could investigate its SCR reactivity. For the DE oxidation (Fig. 7a), the MnO_x/CeO_2/ZSM-5 catalyst shows a higher oxidation activity for DE oxidation than does the MnO_x/ZSM-5 catalyst, indicating the promotion of CeO_2 on oxidation activity. The MnO_x/CeO_2 catalyst shows the lowest T_{99} (180 °C) and CO selectivity, further suggesting its highest oxidation activity. For the NH_3-SCR reaction (Fig. 7b), the MnO_x/CeO_2/ZSM-5 catalyst also shows a higher performance than does the MnO_x/ZSM-5 catalyst. But the MnO_x/ZSM-5 catalyst shows a much higher efficiency for NO_x elimination compared to the MnO_x/CeO_2 catalyst. The MnO_x/CeO_2 catalyst exhibits a very low efficiency for NO_x elimination beyond 250 °C (> T_{99} of DEA oxidation), even producing NO_x owing to the over-oxidized NH_3. The inferior SCR reactivity of the MnO_x/CeO_2 catalyst could be ascribed to the abundant strong oxidation active sites in the MnO_x/CeO_2 catalyst, but lack of essential acid sites for the SCR reaction. However, the co-existence of strong oxidation active sites (from MnO_x) and abundant acid sites (of ZSM-5) in the MnO_x/ZSM-5 catalyst could enable the SCR reaction to undergo smoothly. Moreover, the CeO_2 species further enhances the

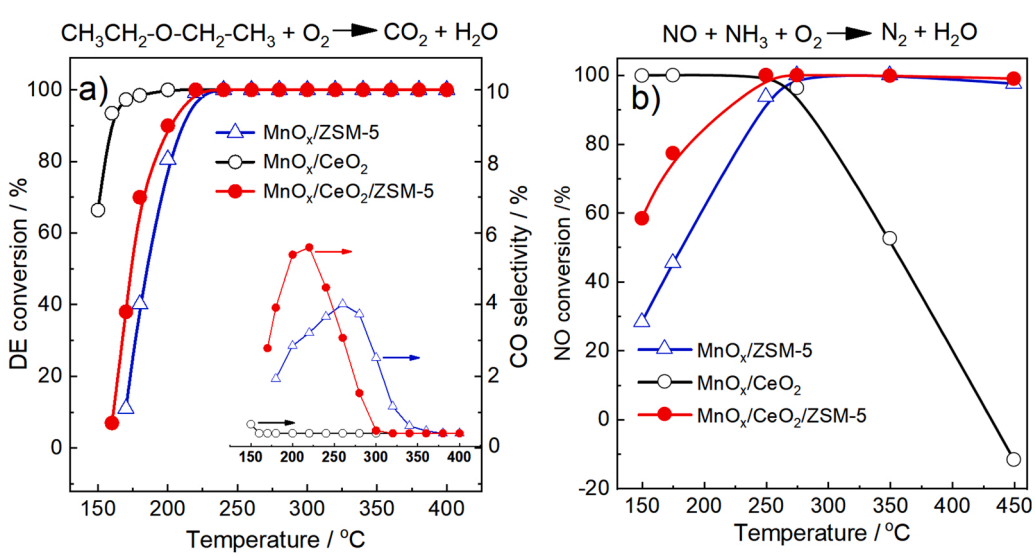

Fig. 7. a) The catalytic oxidation reaction of DE and b) The standard SCR reaction over MnO_x-based catalysts.

oxidation reactivity of the MnO_x/ZSM-5 catalyst, which is related to the increased SCR reactivity and N_2 selectivity for DEA oxidation as observed in the MnO_x/CeO_2/ZSM-5 catalyst.

3.3. Discussion

This work presented the CeO_2-modified MnO_x/ZSM-5 catalysts with high oxidation activity and N_2 selectivity, and broadened $\triangle T$ for DEA oxidation. DEA light-off curves (Fig. 1) suggest the MnO_x species are the dominate oxidation active sites rather than CeO_2 species for DEA oxidation. CeO_2 species could be well dispersed on the ZSM-5 support (as evidenced by XRD, BET and element mapping), MnO_x species prefer to locate on CeO_2 surface in the sequential impregnation method according to the element mapping and surface atomic ratio of Mn/Ce (Table 3) results, and more Mn^{4+} species form on the CeO_2 surface (H_2-TPR and XPS). These observations strongly suggest the interaction of MnO_x with CeO_2, and CeO_2 species markedly modulate the oxidation state of MnO_x. Additionally, the MnO_x/CeO_2/ZSM-5 catalyst exhibits the higher content of Mn^{4+} species in comparison with the MnO_x-CeO_2/ZSM-5 and CeO_2/MnO_x/ZSM-5 catalyst, suggesting the loading sequence of MnO_x and CeO_2 also affects the formation of Mn^{4+} species. Most transition metal oxides catalyzed the VOCs oxidation through MvK reaction mechanism and high oxidation state metal oxides are often regarded as the active sites [32]. Oxidation activities of catalysts for DEA oxidation are ordered as following: MnO_x/CeO_2 > MnO_x/CeO_2/ZSM-5 > MnO_x-CeO_2/ZSM-5 > CeO_2/MnO_x/ZSM-5 > -MnO_x/ZSM-5. This order is in line with that of the content of Mn^{4+} species in catalyst, suggesting Mn^{4+} species as the key oxidation active sites and the possibility of MvK reaction mechanism for DEA oxidation over the MnO_x-based catalysts. For the DE oxidation reaction, the oxidation activities of the representative catalysts are in order of MnO_x/CeO_2 > MnO_x/CeO_2/ZSM-5 > MnO_x/ZSM-5, further confirming Mn^{4+} species as the dominate oxidation active sites.

Mechanism of controlling N_2 selectivity for DEA oxidation is also necessary to be clarified. The MnO_x/CeO_2 catalyst shows the highest oxidation activity but the lowest selectivity to N_2 for DEA oxidation (Fig. 1 and Table 1). Compared to the MnO_x/CeO_2 catalyst, the MnO_x/ZSM-5 catalyst shows a much higher N_2 selectivity for DEA oxidation, which can be ascribed to the abundant acid sites in ZSM-5. In the NH_3-SCR reaction, it is commonly believed that NH_3 is adsorbed and activated on the acid sites to NH_4^+, which is beneficial for NO_x reduction to N_2 ($NH_4^+ + NO_x \rightarrow N_2 + H_2O + H^+$) [38,39]. Both the NH_3-TPD tests and NH_3-SCR model reaction indeed confirm a higher SCR reactivity of the MnO_x/ZSM-5 catalyst than the MnO_x/CeO_2 catalyst. Thus, it is reasonable to infer that acid sites are also very important for the adsorption and activation of the DEA, promoting the internal SCR reaction between NO_x with DEA and generation of N_2. Noticeably, the signals of both NO and N_2 are absent in the NH_3-TPD profile of bare support ZSM-5 (Fig. S1), suggesting the critical role of oxidation active sites (MnO_x or CeO_2) in the both oxidation and SCR reactions. In addition, MnO_x as oxidation active sites have stronger oxidative ability than CeO_2 according to the DEA light-off curves and H_2-TPR (Figs. 1 and 3). Combined with the N_2 signal in NH_3-TPD profiles of the MnO_x/ZSM-5 and CeO_2/ZSM-5 catalysts, it could be inferred that synergistic catalysis of strong oxidation active sites from MnO_x and acid sites from ZSM-5 are indispensable for a high SCR reactivity.

Oxidation state of MnO_x also remarkably affects the SCR reactivity of the catalysts as results given in the NH_3-TPD and NH_3-SCR of the MnO_x/ZSM-5 and MnO_x/CeO_2/ZSM-5 catalysts. Mn^{4+} species with strong oxidation ability are widely recognized as crucial active sites to promote the involved oxidation reaction during the NH_3-SCR reaction (such as oxidation of nitrite to nitrate), thereby accelerating the SCR reaction. Thus, the correlation of ratio of Mn^{4+}/Mn^{3+} in MnO_x-based catalysts with the SCR reactivity have been often discussed in previous works [16, 19,40]. Addition of CeO_2 and its addition sequence significantly affect the ratio of Mn^{4+}/Mn^{3+} of catalyst in this work. MnO_x species mainly locate on the CeO_2 surface in the MnO_x/CeO_2/ZSM-5 catalyst showed the highest ratio of Mn^{4+}/Mn^{3+} in the three CeO_2 modified MnO_x/ZSM-5 catalyst, which should be responsible for its highest oxidation activity and N_2 selectivity, and widest ΔT for high N_2 selectivity. This observation further confirms the above conclusion that synergistic catalysis of strong oxidation active sites and acid sites undergoes the SCR reaction. Although the high content of Ce^{3+} species, as a reactive species for forming oxygen vacancy, is also regraded to be conducive to SCR reaction over CeO_2 based catalyst, the dominate role of MnO_x species can be obviously observed in this work [41]. Therefore, the relationship of ratio of Ce^{3+}/Ce^{4+} with the catalyst performance has not been discussed in detail.

The possible mechanism for the DEA oxidation over the MnO_x/CeO_2/ZSM-5 catalyst has been proposed based on the discussions above (Scheme 1). DEA is firstly over-oxidized by active oxygen species on the surface of the MnO_x/CeO_2/ZSM-5 catalyst to NO_x through MvK mechanism, including production of CO_2 and H_2O. Then, gaseous NO_x reacts with the absorbed DEA by acid sites to produce N_2 through the Eley-Rideal mechanism, which is widely regarded as the dominate pathway for SCR reaction [41–44]. Large amount of strong oxidation active sites (Mn^{4+} species) in the MnO_x/CeO_2/ZSM-5 catalyst is responsible for activating oxygen species, thus improving oxidation activity (decreased T_{99}) of catalyst for DEA oxidation; then the synergistic catalysis of strong oxidation active sites with acid sites, regarded as SCR active sites, accelerates the internal SCR reactivity for the fast reduction of NO_x to N_2, resulting in a high N_2 selectivity. High oxidation state MnO_x is firstly reduced by DEA and then re-oxidized by the gaseous oxygen, thus achieving the cycle of lattice oxygen as oxidation sites. Therefore, the multi-active sites, oxidation active sites and SCR active sites, are both crucial for a catalyst with high oxidation activity and N_2 selectivity for DEA oxidation.

Water tolerance is of great importance for the applied catalysts, thus the effect of water steam on the catalytic performance of the MnO_x/CeO_2/ZSM-5 catalyst has been investigated (Fig. 8). It can be seen that water steam in the feed gas has no influence on the oxidation activity for DEA oxidation over the MnO_x/CeO_2/ZSM-5 catalyst, and water steam even promotes the increase of N_2 selectivity at high reaction temperature which is also observed in the reaction system of CuO/SSZ-13 catalyzing DEA oxidation [13]. CO byproduct slightly increase under wet reaction condition, suggesting the only a few active sites for CO oxidation are covered by water steam. The above result confirms the potential application of the MnO_x/CeO_2/ZSM-5 catalyst.

4. Conclusion

In summary, the MnO_x/CeO_2/ZSM-5 catalyst with multi-active sites,

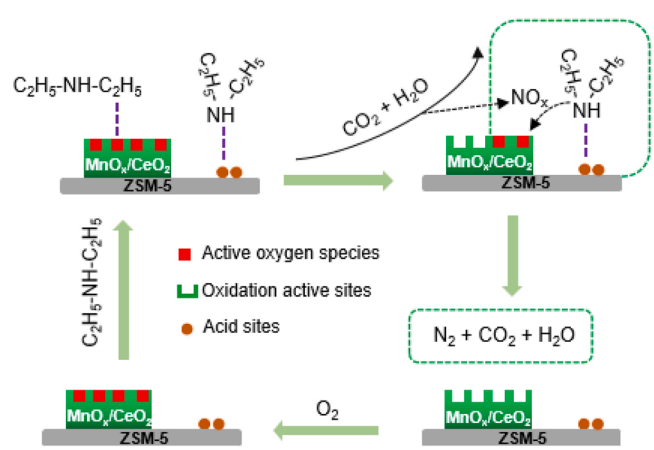

Scheme 1. The proposed mechanism for the DEA oxidation over the MnO_x/CeO_2/ZSM-5 catalyst.

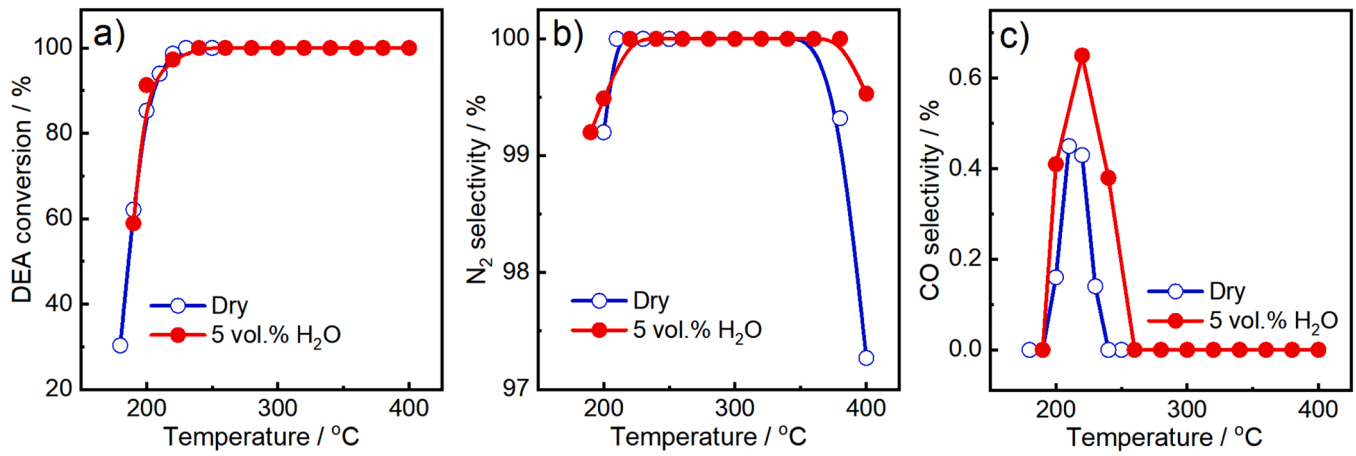

Fig. 8. The catalytic performance of the MnO_x/CeO_2/ZSM-5 catalyst for DEA oxidation under dry and wet (5 % H_2O) conditions.

oxidation active sites and SCR active sites, has been successfully prepared for DEA selective catalytic oxidation. It is found that Mn^{4+} species are the dominate oxidation active sites, and the addition of CeO_2 into the MnO_x/ZSM-5 catalyst remarkably improves the ratio of Mn^{4+} species. It is further found that the MnO_x/CeO_2/ZSM-5 catalyst with the most abundant Mn^{4+} species shows the highest oxidation activity in all three CeO_2-modified MnO_x/ZSM-5 catalysts for the DEA oxidation. Furthermore, the synergistic catalysis of strong oxidation active sites (from MnO_x species) and acid sites (from ZSM-5) accelerates the internal SCR reaction of NO_x from over-oxidized DEA on the catalyst surface, thereby increasing the N_2 selectivity of catalyst for DEA oxidation. Therefore, the surface active sites of the MnO_x/ZSM-5 catalyst could be modulated by adding CeO_2 or changing its addition sequence for selective catalytic oxidation of DEA.

CRediT authorship contribution statement

Lin-Cong He: Conceptualization, Data curation, Formal analysis, Investigation, Software, Visualization, Writing – original draft. **Xu-Fang Wang:** Conceptualization, Data curation, Formal analysis, Investigation. **Chu-Feng Liu:** Investigation, Data curation, Formal analysis, Visualization. **Bei Li:** Conceptualization, Investigation, Resources, Data curation, Funding acquisition. **Meng-Fei Luo:** Conceptualization, Data curation, Formal analysis, Funding acquisition, Investigation, Methodology, Resources, Project administration, Supervision, Writing – review & editing. **Jian Chen:** Conceptualization, Data curation, Formal analysis, Investigation, Visualization, Software, Methodology, Supervision, Writing – review & editing.

Declaration of Competing Interest

The authors declare that they have no known competing financial interests or personal relationships that could have appeared to influence the work reported in this paper.

Data Availability

Data will be made available on request.

Acknowledgements

This work was financially supported by the Natural Science Foundation of Zhejiang Province, China (No. LY21B030004) and the National Natural Science Foundation of China (Nos. 22172145, 21902146). We highly appreciate Professor Xuesong Liu (Shaoxing University) for the help in NH_3-SCR reaction and Peifang Yan (Dalian Institute of Chemical Physics) for the assistance in the NH_3-TPD analysis experiments.

Appendix A. Supporting information

Supplementary data associated with this article can be found in the online version at doi:10.1016/j.apcata.2022.118929.

References

[1] R. Zhang, N. Liu, Z. Lei, B. Chen, Selective transformation of various nitrogen containing exhaust gases toward N_2 over zeolite catalysts, Chem. Rev. 116 (2016) 3658–3721.
[2] M. Ma, Y. Jian, C. Chen, C. He, Spherical-like Pd/SiO_2 catalysts for n-butylamine effffffficient combustion: effect of support property and preparation method, Catal. Today 339 (2020) 181–191.
[3] N. Liu, X. Yuan, R. Zhang, R. Xu, Y. Li, Mechanistic insight into selective catalytic combustion of acrylonitrile (C_2H_3CN): NCO formation and its further transformation towards N_2, Phys. Chem. Chem. Phys. 19 (2017) 7971–7979.
[4] Y.Y. Zhang, Y.X. Wang, Y. Liu, Q.J. Ying, Z.B. Wu, Catalytic combustion of acetonitrile over $CuCeO_x$-HZSM-5 composite catalysts with different mass ratios: the synergism between oxidation and hydrolysis reactions, J. Colloid Interface Sci. 584 (2021) 193–203.
[5] M. Ma, H. Huang, C. Chen, Q. Zhu, L. Yue, R. Albilali, C. He, Highly active SBA-15-confined Pd catalyst with short rod-like micromesoporous hybrid nanostructure for n-butylamine low-temperature destruction, Mol. Catal. 455 (2018) 192–203.
[6] T. Nanba, S. Masukawa, J. Uchisawa, A. Obuchi, Screening of catalysts for acrylonitrile decomposition, Catal. Lett. 93 (2004) 195–201.
[7] N. Liu, D.J. Shi, R.D. Zhang, Y.X. Li, B.H. Chen, Highly selective catalytic combustion of acrylonitrile towards nitrogen over Cu-modified zeolites, Catal. Today 332 (2019) 201–213.
[8] L.F. Liotta, Catalytic oxidation of volatile organic compounds on supported noble metals, Appl. Catal. B Environ. 100 (2010) 403–412.
[9] D.D. Li, X.Y. Leng, X.F. Wang, H.B. Yu, W.Q. Zhang, J. Chen, J.Q. Lu, M.F. Luo, Unraveling the promoting roles of sulfate groups on propane combustion over Pt-SO_4^{2-}/ZrO_2 catalysts, J. Catal. 407 (2022) 322–332.
[10] B.H. Cen, C. Tang, J.Q. Lu, J. Chen, M.F. Luo, Different roles of MoO_3 and Nb_2O_5 promotion in short-chain alkane combustion over Pt/ZrO_2 catalysts, Chin. J. Catal. 42 (2021) 2287–2295.
[11] W.X. Zhang, S. Xia, C.L. Chen, H.H. He, Z.N. Jin, M.F. Luo, J. Chen, Understanding the crucial roles of catalyst properties in ethyl acetate and toluene oxidation over Pt catalysts, New J. Chem. 45 (2021) 11352–11358.
[12] X.L. Wei, S. Wang, D.K. Xu, S.D. Wang, Mechanistic insights on the reaction behaviors of the acrylonitrile selective catalytic combustion over Cu-based UZM-9, J. Hazard. Mater. 392 (2020), 122497.
[13] X.Y. Leng, W.Y. Wang, L.C. He, D.D. Li, J. Chen, M.F. Luo, Novel insights into diethylamine catalytic combustion over CuO catalysts supported by SSZ-13: undesirable product NO_x as a crucial intermediate for N_2 generation, Mol. Catal. 516 (2021), 111952.
[14] Y. Lu, C. Hu, W. Zhang, Z. Jin, X. Leng, Y. Wang, J. Chen, M. Luo, Promoting the selective catalytic oxidation of diethylamine over MnO_x/ZSM-5 by surface acid centers, Appl. Surf. Sci. 521 (2020), 146348.
[15] C.H. Hu, C.T. Fang, Y. Lu, Y.J. Wang, J. Chen, M.F. Luo, Selective oxidation of diethylamine on CuO/ZSM-5 catalysts: the role of cooperative catalysis of CuO and surface acid sites, Ind. Eng. Chem. Res. 59 (2020) 9432–9439.
[16] S. Liu, Y.J. Ji, W.Q. Xu, J.L. Zhang, R.H. Jiang, L. Li, L.H. Jia, Z.Y. Zhong, G.W. Xu, T.Y. Zhu, F.B. Su, Hierarchically interconnected porous $Mn_xCo_{3-x}O_4$ spinels for low temperature catalytic reduction of NO by CO, J. Catal. 406 (2022) 72–86.
[17] X. Liu, X. Wu, D. Weng, L. Shi, Modification of Cu/ZSM-5 catalyst with CeO_2 for selective catalytic reduction of NO_x with ammonia, J. Rare Earths 34 (2016) 1004–1009.

[18] Y. Wang, Q.J. Ying, Y.Y. Zhang, Y. Liu, Z.B. Wu, Reaction behaviors of CH_3CN catalytic combustion over $CuCeO_x$-HZSM-5 composite catalysts: the mechanism of enhanced N_2 selectivity, Appl. Catal. A Gen. 590 (2020), 117373.

[19] X. Yao, L. Chen, J. Cao, Y. Chen, M. Tian, F.M. Yang, J.F. Sun, C.J. Tang, L. Dong, Enhancing the $deNO_x$ performance of MnO_x/CeO_2-ZrO_2 nanorod catalyst for low-temperature NH_3-SCR by TiO_2 modification, Chem. Eng. J. 369 (2019) 46–56.

[20] C. Liu, J.W. Shi, C. Gao, C. Niu, Manganese oxide-based catalysts for low-temperature selective catalytic reduction of NO_x with NH_3: a review, Appl. Catal. A Gen. 522 (2016) 54–69.

[21] T. Qiao, Z.G. Liu, C.H. Liu, W. Meng, H. Sun, Y. Lu, MnO_x location on MnO_x-ZSM-5 to influence the catalytic activity for selective catalytic reduction of NO_x by NH_3, Appl. Catal. A Gen. 617 (2021), 118128.

[22] F. Kapteljn, L. Smgoredjo, A. Andreini, Activity and selectivity of pure manganese oxides in the selective catalytic reduction of nitric oxide with ammonia, Appl. Catal. B Environ. 3 (1994) 173–189.

[23] W.P. Shan, F.D. Liu, H. He, X.Y. Shi, C.B. Zhang, A superior Ce-W-Ti mixed oxide catalyst for the selective catalytic reduction of NO_x with NH_3, Appl. Catal. B Environ. 115–116 (2012) 100–106.

[24] M.Y. Lin, B.X. An, N. Niimi, Y. Jikihara, T. Nakayama, T. Honma, T. Takei, T. Shishido, T. Ishida, M. Haruta, T. Murayama, Role of the acid site for selective catalytic oxidation of NH_3 over Au/Nb_2O_5, ACS Catal. 9 (2019) 1753–1756.

[25] F. Gao, N.M. Washton, Y.L. Wang, M. Kollár, J. Szanyi, C.F. Peden, Effects of Si/Al ratio on Cu/SSZ-13 NH_3-SCR catalysts: implications for the active Cu species and the roles of Brønsted acidity, J. Catal. 331 (2015) 25–38.

[26] J. Quiroz, J. Giraudon, A. Gervasini, C. Dujardin, C. Lancelot, M. Trentesaux, J. Lamonier, Total oxidation of formaldehyde over MnO_x-CeO_2 catalysts: the effect of acid treatment, ACS Catal. 5 (2015) 2260–2269.

[27] X.F. Tang, J.H. Li, L. Sun, J. Hao, Origination of N_2O from NO reduction by NH_3 over β-MnO_2 and α-Mn_2O_3, Appl. Catal. B Environ. 99 (2010) 156–162.

[28] L. Katta, P. Sudarsanam, G. Thrimurthulu, B.M. Reddy, Doped nanosized ceria solid solutions for low temperature soot oxidation: zirconium versus lanthanum promoters, Appl. Catal. B Environ. 101 (2010) 101–108.

[29] X.L. Guo, R.X. Zhou, A new insight into the morphology effect of ceria on CuO/CeO_2 catalysts for CO selective oxidation in hydrogen-rich gas, Catal. Sci. Technol. 6 (2016) 3862–3871.

[30] R. Leppelt, B. Schumacher, V. Plzak, V. Plzak, M. Kinne, R. Behm, Kinetics and mechanism of the low-temperature water-gas shift reaction on Au/CeO_2 catalysts in an idealized reaction atmosphere, J. Catal. 244 (2006) 137–152.

[31] X. Guo, R. Zhou, A new insight into the morphology effect of ceria on CuO/CeO_2 catalysts for CO selective oxidation in hydrogen-rich gas, Catal. Sci. Technol. 6 (2016) 3862–3871.

[32] C.F. Liu, L.C. He, X.F. Wang, J. Chen, J.Q. Lu, M.F. Luo, Tailoring Co_3O_4 active species to promote propane combustion over Co_3O_4/ZSM-5 catalyst, Mol. Catal. 524 (2022), 112297.

[33] C.T. Fang, D.D. Li, X.F. Wang, Y.J. Wang, J. Chen, M.F. Luo, Exploring an efficient manganese oxide catalyst for ozone decomposition and its deactivation induced by water vapor, New J. Chem. 45 (2021) 10402–10408.

[34] W.Y. Wang, D.D. Li, H.B. Yu, C.F. Liu, C. Tang, J. Chen, J.Q. Lu, M.F. Luo, Insights into different reaction behaviors of propane and CO oxidation over Pt/CeO_2 and Pt/Nb_2O_5: The crucial roles of support properties, J. Phys. Chem. C 125 (2021) 19301–19310.

[35] B. Cen, W. Wang, P. Zhao, C. Liu, J. Chen, J. Lu, M. Luo, Revealing the different roles of sulfates on Pt/Al_2O_3 catalyst for methane and propane combustion, Catal. Lett. 152 (2022) 863–871.

[36] M. Bendrich, A. Scheuer, R.E. Hayes, M. Votsmeier, Unified mechanistic model for standard SCR, fast SCR, and NO_2 SCR over a copper chabazite catalyst, Appl. Catal. B Environ. 222 (2018) 76–87.

[37] T. Nanba, S. Masukawa, A. Ogata, J. Uchisawa, A. Obuchi, Active sites of Cu-ZSM-5 for the decomposition of acrylonitrile, Appl. Catal. B Environ. 61 (2005) 288–296.

[38] R.Q. Long, R.T. Yang, Superior Fe-ZSM-5 catalyst for selective catalytic reduction of nitric oxide by ammonia, J. Am. Chem. Soc. 121 (1999) 5595–5596.

[39] A.L. Kustov, T.W. Hansen, M. Kustova, C.H. Christensen, Selective catalytic reduction of NO by ammonia using mesoporous Fe-containing HZSM-5 and HZSM-12 zeolite catalysts: an option for automotive applications, Appl. Catal. B Environ. 76 (2007) 311–319.

[40] S.C. Deng, T.T. Meng, B.L. Xu, F. Gao, Y.H. Ding, L. Yu, Y.N. Fan, Advanced MnO_x/TiO_2 catalyst with preferentially exposed anatase {001} facet for low-temperature SCR of NO, ACS Catal. 6 (9) (2016) 5807–5815.

[41] D.M. Meng, W.C. Zhan, Y. Guo, Y.L. Guo, L. Wang, G.Z. Lu, A highly effective catalyst of sm-MnO_x for the NH_3-SCR of NO_x at low temperature: promotional role of sm and its catalytic performance, ACS Catal. 5 (2015) 5973–5983.

[42] D. Kim, Y. Park, K. Lee, H. Ha, D. Kwon, Surface insights into MnO_x-based catalysts containing metal oxides for the selective catalytic reduction of NO_X with NH_3, Appl. Catal. A Gen. 643 (2022), 118770.

[43] H.Y. Xue, X.M. Guo, T. Meng, Q.S. Guo, D.S. Mao, S. Wang, Cu-ZSM-5 catalyst impregnated with Mn-Co oxide for the selected catalytic reduction of NO: physicochemical property-catalytic activity relationship and In Situ DRIFTS study for the reaction mechanism, ACS Catal. 11 (2021) 7702–7718.

[44] J.C. Mu, X.Y. Li, W.B. Sun, S.Y. Fan, X.Y. Wang, L. Wang, M.C. Qin, G.Q. Gan, Z. F. Yin, D.K. Zhang, Inductive effect boosting catalytic performance of advanced $Fe_{1-x}V_xO_8$ catalysts in low-temperature NH_3 selective catalytic reduction: insight into the structure, interaction, and mechanisms, ACS Catal. 8 (2018) 6760–6774.